Cardiolipin Affects the Supramolecular Organization of ATP Synthase in Mitochondria

Devrim Acehan,[†‡] Ashim Malhotra,[§] Yang Xu,[§] Mindong Ren,[†] David L. Stokes,[†‡¶] and Michael Schlame[†§*]
[†]Department of Cell Biology, [‡]Skirball Institute, Structural Biology Program, and [§]Department of Anesthesiology, New York University School of Medicine, New York, New York; and [¶]New York Structural Biology Center, New York, New York

ABSTRACT F_1F_0 ATP synthase forms dimers that tend to assemble into large supramolecular structures. We show that the presence of cardiolipin is critical for the degree of oligomerization and the degree of order in these ATP synthase assemblies. This conclusion was drawn from the statistical analysis of cryoelectron tomograms of cristae vesicles isolated from *Drosophila* flight-muscle mitochondria, which are very rich in ATP synthase. Our study included a wild-type control, a cardiolipin synthase mutant with nearly complete loss of cardiolipin, and a tafazzin mutant with reduced cardiolipin levels. In the wild-type, the high-curvature edge of crista vesicles was densely populated with ATP synthase molecules that were typically organized in one or two rows of dimers. In both mutants, the density of ATP synthase was reduced at the high-curvature zone despite unchanged expression levels. Compared to the wild-type, dimer rows were less extended in the mutants and there was more scatter in the orientation of dimers. These data suggest that cardiolipin promotes the ribbonlike assembly of ATP synthase dimers and thus affects lateral organization and morphology of the crista membrane.

INTRODUCTION

In the mitochondrial inner membrane, a specific phospholipid, cardiolipin, is thought to play a pivotal role in overall membrane organization and dynamics (1–4). However, little is known about the impact of cardiolipin on the organization of mitochondrial membrane components, except for the fact that this phospholipid has been shown to bind rather tightly to certain protein surfaces. This has been demonstrated by ^{31}P NMR of endogenous cardiolipin in purified preparations of the mitochondrial ADP-ATP carrier (5) and the mitochondrial ATP synthase (6), but it is probably true for other mitochondrial proteins as well. Cardiolipin has also been shown to affect protein conformation (7) and folding (8), which suggests intriguing roles comparable to those of molecular chaperones.

The Δ*crd1* mutant of yeast, in which the final step of cardiolipin biosynthesis is deleted, has been used extensively to study the biological function of cardiolipin (9). In this mutant, the assembly of components of the respiratory chain into supercomplexes is diminished (10,11) as is the association of respiratory supercomplexes with the ADP-ATP carrier (12), suggesting that cardiolipin promotes the clustering of protein complexes. An observed decrease in the ADP/oxygen ratio and the respiratory control ratio in mitochondria isolated from Δ*crd1* yeast supports the idea that cardiolipin enhances the overall efficiency of energy transformation by promoting respiratory supercomplexes (12,13).

In higher organisms, mitochondria may have special features that enable them to cope with tissue-specific high-energy demands or metabolic activities. Such mitochondria may be dependent on efficient energy transformation and thus be even more sensitive to the lack of cardiolipin than yeast mitochondria. For example, indirect flight muscle of *Drosophila* is able to sustain wing beat frequencies of over 100/s. Consequently, it has abundant mitochondria and those mitochondria have a high concentration of tightly packed cristae. We chose flight-muscle mitochondria to investigate the role of cardiolipin in the organization of the ATP synthase, an enzyme that is thought to have dual functions in energy metabolism and crista structure. ATP synthase has been shown to form dimers (14,15), as well as higher oligomeric assemblies, i.e., dimer rows (16–18), and the oligomeric arrangement of ATP synthase has been implicated in shaping the cristae (18). Although cardiolipin did not seem to be essential for dimerization per se (11), it is not known whether cardiolipin has any effect on the long-range supramolecular organization of the ATP synthase. In this article, we employed cryoelectron tomography to compare the structural organization of the ATP synthase in flight-muscle mitochondria from wild-type and cardiolipin-synthase mutant flies with virtually complete loss of cardiolipin. Our data reveal a novel function of cardiolipin, what we believe is modulation of the long-range assembly state of ATP synthase.

MATERIALS AND METHODS

Drosophila strains and physiologic assays

Strain w^{1118}; PBac{PB} CG4774^{c01874}/TM6B, Tb^1, with a transposon insertion in the coding region of the last exon of the cardiolipin synthase gene (ΔCLS), was obtained from the Bloomington *Drosophila* Stock Center (No. 10741). The tafazzin mutant (ΔTAZ) was created in our laboratory (19). Flies were grown in 3-inch culture vials on a standard

Submitted December 16, 2010, and accepted for publication March 28, 2011.

*Correspondence: michael.schlame@med.nyu.edu

Editor: Robert Nakamoto.

0006-3495/11/05/2184/9 $2.00

doi: 10.1016/j.bpj.2011.03.031

cornmeal-sucrose-yeast medium. All physiologic assays were conducted in age-synchronized fly populations at room temperature. Locomotor activity of third instar larvae was measured on agar dishes placed on a grid. We determined the number of 1/4-inch × 1/4-inch squares crossed within 5 min. The heart rate of early pupae was measured under a light microscope. Climbing activity was determined in adult flies by measuring the distance that flies climbed within a 12-s interval. Flies were collected at the bottom of the tube and allowed to climb for 12 s. A picture was taken after this interval, and the distribution of the fly population across the tube was determined from the photograph. Data are presented in bar graphs as means ± SE. Kaplan-Meier analysis was used to determine longevity.

Electron microscopy of chemically fixed samples

Partially dissected fruit flies were conventionally fixed using glutaraldehyde and osmium tetroxide. The fixed tissues were stained with uranyl acetate, and the buffer was then gradually exchanged with ethanol, followed by resin exchange and heat polymerization in epoxy resin. Sections (50–100 nm) were cut and collected on EM grids, stained with uranyl acetate and Sato Lead stains, and finally imaged with a CM12 electron microscope. Tomography of flight-muscle mitochondria was performed as described before (20).

Isolation of mitochondria from *Drosophila* flight muscle

Mitochondria were isolated from fly thoraces, in which flight muscle is the most abundant tissue. For each mitochondrial preparation, ~100 flies were immobilized by cooling on ice. Thoraces were dissected under a microscope and then placed in ice-cold isolation buffer (0.28 M sucrose, 0.01 M Tris, and 0.25 mM EDTA, pH 7.3 at 4°C). All subsequent steps were also performed in ice-cold medium. Thoraces were homogenized with a tight-fitting Teflon-glass homogenizer, the volume was adjusted to 30 ml with isolation medium, and the homogenate was spun at 750 *g* for 5 min. The supernatant was collected, filtered through gauze, and then spun again at 750 *g* for 5 min. The supernatant was collected and filtered again. Next, the supernatant was spun at 8000 *g* for 10 min to sediment mitochondria. Mitochondria were resuspended in isolation medium using a loose-fitting glass-glass homogenizer. Protein concentration of mitochondria was determined by the method of Lowry (21). The protein yields typically ranged from 0.5 to 1.0 mg. Mitochondria from whole flies were isolated by the same method.

Cryoelectron tomography

Mitochondrial suspensions (protein concentration 5 mg/ml) were gently sonicated using a 10-s burst delivered by a microtip. Sonicated mitochondria were collected by centrifugation in a table-top centrifuge and aliquots of the resuspended mitochondria were plunge-frozen on holey carbon EM grids in liquid ethane cooled by liquid nitrogen. We imaged mitochondrial fragments in vitreous ice over holes in a 300-kV Jeol electron microscope equipped with an energy filter. Single tilt-axis images were collected from -60° to +60° at 2° intervals with an estimated total dose of 60 e^-/A^2. Sample features were used for cross-correlation by the FSU tomogram reconstruction package (22). After tomograms were formed, we segmented membranes and the characteristic globular F_1 domains of the ATP synthase complexes.

Analysis of tomograms

We determined the spatial coordinates of the segmented F_1 domains and used these coordinates for distance measurements and other statistical analyses. Initially, we determined distances between F_1-F_1 pairs by Pythagorean relations. This analysis included all possible F_1-F_1 pairs for which the connecting line did not pass through the vesicle membrane. Next, we performed near-neighbor analyses for each F_1 particle, starting with the closest neighbor. In this step, we rejected prospective neighbors if the connecting line crossed another closer neighbor, i.e., if the two connecting lines formed an angle of 5° or less. In this fashion, we could assign to each particle a set of neighbors ranked by their distance from that particle.

Lipid analysis

Mitochondria were isolated from whole flies, using the same protocol as described above. Lipids were extracted into chloroform/methanol (23) from aliquots corresponding to 2 mg mitochondrial protein. Phospholipids were separated by two-dimensional thin-layer chromatography and digested by 70% perchloric acid, followed by colorimetric assay of phosphorus (24). Alternatively, lipids were separated on a Hypersil (Thermo, Waltham, MA) silica high-performance liquid chromatography column (100 × 4.6 mm) developed with acetonitrile-water containing 0.025% ammonia. A gradient was run changing the water concentration from 1% to 10% over 30 min (flow rate 1.0 ml/min). Acidic phospholipids (retention times 5–10 min) were collected, dried under a stream of nitrogen, and resuspended in 50 μl chloroform/methanol (1:1). Aliquots of these samples were diluted 1:10 in 2-propanol-acetonitrile (3:2) to perform MALDI-TOF mass spectrometry as described by Sun et al. (25), using 9-aminoacridine as matrix. Spectra were recorded in negative ion mode with a MALDI micro MX mass spectrometer from Waters (Wilmslow, UK). The instrument was operated in reflectron mode, the pulse voltage was set to 2000 V, and the detector voltage was set to 2400 V. Spectra were obtained by averaging 1000 laser shots (10 shots per subspectrum, 100 subspectra).

Two-dimensional blue-native/sodium dodecyl sulfate-polyacrylamide gel electrophoresis (2D-BN/SDS-PAGE)

Isolated *Drosophila* mitochondria (200 μg protein) were solubilized by digitonin (6 g digitonin/1 g protein) and subsequently separated by BN-PAGE on a 4–13% acrylamide gradient gel (26). Gel strips were excised, soaked in 1% SDS, and then embedded on top of the SDS-PAGE gel for electrophoretic separation in the second dimension. Proteins were transferred to PVDF membranes and Western blotting was performed with a primary antibody to the α-subunit of ATP synthase (MitoSciences, Eugene, OR) at a concentration of 1 μg/ml in Odyssey blocking buffer (LI-COR Biosciences, Lincoln, NE). IRDye 680 (Li-Cor Biosciences) was used as secondary antibody and the fluorescence patterns of the blots were analyzed by a Li-Cor scanner. We also performed conventional Western blotting with secondary horseradish-peroxidase-conjugated anti-mouse antibody and SuperSignal peroxidase substrate from Pierce.

RESULTS

ATP synthase forms two parallel rows of dimers at the high-curvature apex of mitochondrial crista vesicles

Mitochondria were isolated from *Drosophila* thoraces, in which flight muscle constitutes the bulk of the tissue mass. The mitochondrial preparations showed excellent ultrastructural preservation and the isolated organelles maintained the high crista density that is characteristic of flight-muscle mitochondria (19,27) (Fig. S1 in the Supporting Material). Mitochondria were disrupted by mild

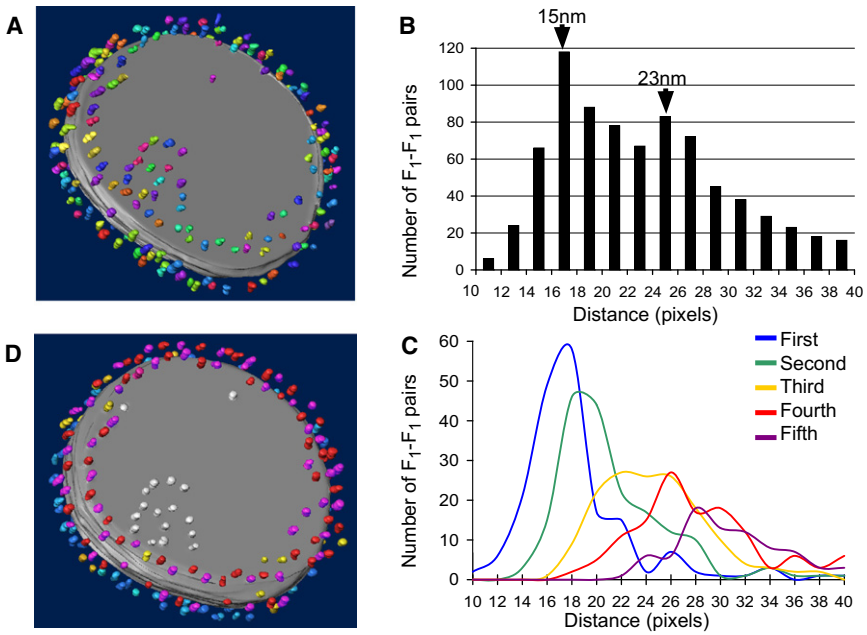

FIGURE 1 State of oligomerization of ATP synthase. (*A*) 3-D model of a tomogram of a membrane vesicle. F_1 particles ($n = 187$) are shown in random colors and the membrane surface is shown in gray. F_1 particles are concentrated at the high-curvature zone of the disc-shaped vesicle. (*B*) Distance histogram of F_1-F_1 pairs. The histogram includes all F_1-F_1 pairs for which the connecting line does not intersect with another F_1 particle (see Methods section for details). The distance population peaks at 15 nm and at 23 nm (1 pixel = 8.83 Å). (*C*) Separate distance histograms are shown for the closest neighbor (*blue*), the second closest neighbor (*green*), the third closest neighbor (*yellow*), the fourth closest neighbor (*red*), and the fifth closest neighbor (*purple*). The histogram data points are curve-fitted to enhance clarity. (*D*) 3-D model of Fig. 1 *A* rendered in different colors. Dimers are colored in alternating shades of red or blue, revealing two parallel dimer rows on opposite sides of the edge of the disc-shaped vesicle. The surface of the vesicle is colored gray. F_1 particles on the flat surface of the vesicle are colored white and F_1 particles that could not be assigned to any dimer are colored yellow.

sonication, plunge-frozen, and analyzed by cryo-electron tomography, largely following the protocol of Strauss et al. (18). Most of the mitochondrial fragments formed round, disk-shaped vesicles with a diameter of 50–300 nm, reflecting the natural shape and size of cristae in flight-muscle mitochondria in vivo (Fig. S2). Like Strauss et al. (18), we found that the F_1 heads of ATP synthase complexes were clearly visible as 9-nm densities on the surfaces of vesicles derived from the inner membrane (Fig. S3). We resolved the central stalk of the ATP synthase in most complexes and the peripheral stalk in some complexes. However, rather than focusing on the fine structure of the complex, we took advantage of the extraordinary abundance of ATP synthase complexes in flight-muscle mitochondria to study their supramolecular organization.

We were able to approach the problem of supramolecular organization by statistical analysis of the spatial distribution pattern of the F_1 particles (Fig. 1). For instance, the tomogram model depicted in Fig. 1 *A* shows a total of 187 F_1 particles on a single crista vesicle. To be unbiased, we considered any F_1-F_1 pair as a candidate for physical interaction unless it was blocked by a closer neighbor. To analyze the spatial distribution pattern, we measured the center coordinates of all F_1 domains and calculated a matrix of F_1-F_1 distances. The resulting distance histogram showed two peaks, one at 15 nm and another at 23 nm (Fig. 1 *B*). We then analyzed the distances to neighboring particles starting with the closest neighbor, moving to the second closest neighbor, and so on. First and second closest neighbors of a particle had a similar distance within a narrow range of 15–18 nm, whereas the third, fourth, and fifth closest neighbors were 20–30 nm away (Fig. 1 *C*). The distances to the first and second closest neighbors were most conserved

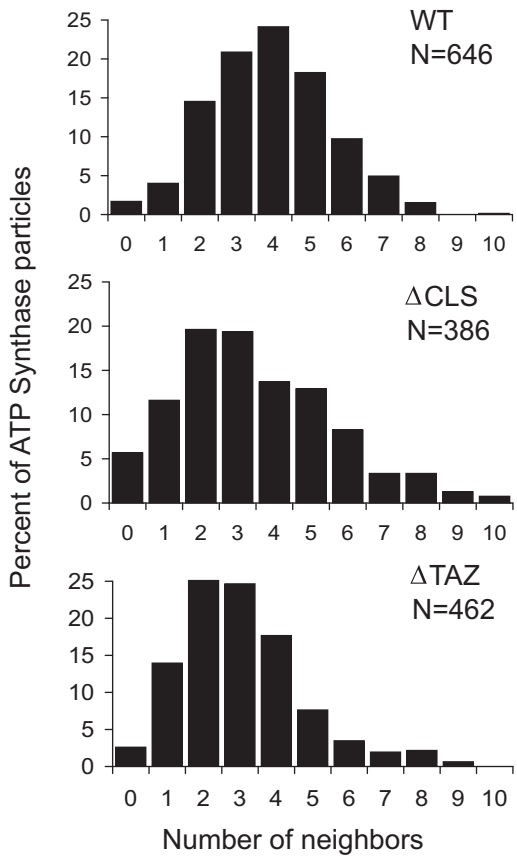

FIGURE 2 Histograms showing (*top* to *bottom*) the number of neighbors per F_1 particle for wild-type flies (*WT*), cardiolipin synthase mutant flies (Δ*CLS*), and tafazzin mutant flies (Δ*TAZ*). A particle was considered the neighbor of another particle if their distance was within 27 nm and if there was no other particle between the two.

throughout the set and fell into the range of interdimer spacings previously observed in mammals, Paramecium, yeast, and Neurospora (16–18,28).

Next, we expanded our analysis to include more membrane vesicles and so were able to collect the spatial coordinates of 646 ATP synthase molecules. In this population, we determined the number of neighbors per ATP synthase molecule within a radius of 27 nm. This radius was chosen because it included both peaks of our distance histogram (Fig. 1 *B*), as well as the published F_1-F_1 distance within a dimer (17,18). Our analysis demonstrated the presence of 0–8 neighbors/F_1 monomer, with an average number of 4 (Fig. 2, *upper*). We concluded that the average ATP synthase molecule has four neighbors, two of them in close proximity and two farther away. These data are compatible with a ribbonlike assembly of ATP synthase dimers (dimer row), but they are incompatible with a number of other theoretical structural arrangements (Fig. S4).

In conclusion, the statistical analysis is consistent with extended ribbonlike assemblies of ATP synthase complexes that approximate a row of dimers. The data also demonstrate to what extent deviations from the ideal structure, e.g., the presence of isolated monomers or multimeric ATP synthase clusters, occur. Ribbons of ATP synthase dimers have been described before in fragmented mitochondria from mammals (18), *Paramecium* (16), *Neurospora* (28), and yeast (17). More recently, they have been observed in intact mitochondria from *Polytomella* (29) and Δfcj1 yeast mutants (30). In *Drosophila* flight muscle, the ATP synthase formed not only one but two rows of dimers, presumably to accommodate the high number of complex molecules. F_1 particles corresponding to first and second dimer rows were color coded for clarity and are shown in Fig. 1 *D* and movie in the Supporting Material. Both dimer rows run parallel at the high-curvature edge of the disc-shaped crista vesicles. In contrast, the ATP synthases on the flat surface of the vesicles were less organized.

Cardiolipin deficiency disrupts the long-range assembly pattern of ATP synthase in flight-muscle mitochondria

We studied the supramolecular organization of ATP synthase in a *Drosophila* strain with a transposon insertion in the gene encoding cardiolipin synthase (CLS, *Drosophila* gene CG4774). As expected, this mutation (ΔCLS) resulted in virtually complete loss of cardiolipin and compensatory increase of phosphatidylglycerol as shown by MALDI-TOF mass spectrometry (Fig. 3 *A*). No other changes in phospholipid composition were noted. When concentrated lipid extracts from mitochondria were analyzed by 2-D thin-layer chromatography, a trace of cardiolipin remained detectable, suggesting residual CLS activity. However, quantitative analysis by phosphorus assay confirmed that cardiolipin was almost completely replaced by phosphatidylglycerol and that the concentration of other mitochondrial phospholipids remained unaltered (Fig. 3 *B*). Although this has been achieved before in cell cultures (31–33), the ΔCLS *Drosophila* strain is the first animal model with nearly complete loss of cardiolipin. The

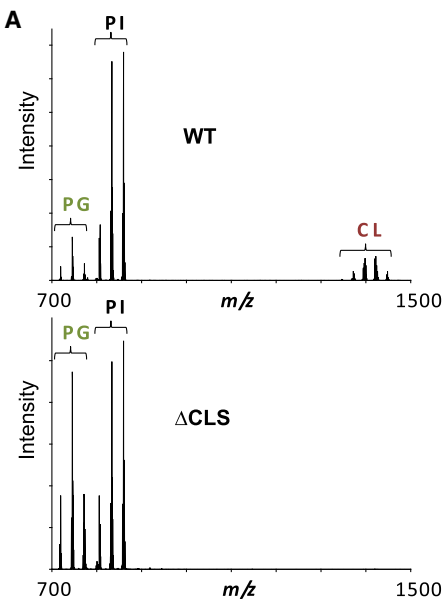

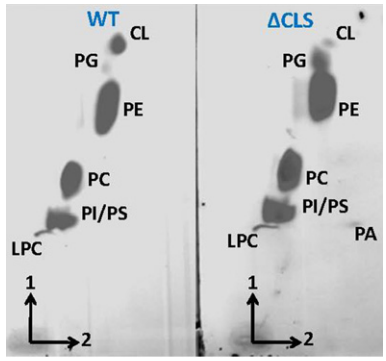

Phospholipid	WT	ΔCLS
PE	47.6±7.1	50.3±2.2
PC	22.6±1.0	27.1±3.5
PI+PS+LPC	25.9±9.2	19.9±5.7
CL	3.7±1.4	Tr
PG	Tr	2.7±0.1
PA	ND	Tr

FIGURE 3 Lipid analysis in ΔCLS *Drosophila*. (*A*) Lipids were extracted from wild-type flies (*WT*) and from cardiolipin synthase mutant flies (Δ*CLS*) and then underwent HPLC separation. The fractions containing acidic phospholipids were collected and analyzed by MALDI-TOF mass spectrometry in negative ion mode. Mutation of CLS causes a decrease in cardiolipin and an increase in phosphatidylglycerol. The principle peaks include (*left* to *right*) palmitoyl-palmitoleoyl-PG (*m/z* = 719.5), palmitoleoyl-oleoyl-PG (*m/z* = 745.5), oleoyl-linoleoyl-PG (*m/z* = 771.5), dipalmitoleoyl-PI (*m/z* = 805.5), palmitoleoyl-oleoyl-PI (*m/z* = 833.5), oleoyl-linoleoyl-PI (*m/z* = 859.5), $(C16)_3$-C18-CL cluster (*peak at m/z* = 1372), $(C16)_2$-$(C18)_2$-CL cluster (*peak at m/z* = 1398), C16-$(C18)_3$-CL cluster (*peak at m/z* = 1422), $(C18)_4$-CL cluster (*peak at m/z* = 1448). (*B*) Mitochondria were isolated from wild-type flies (*WT*) and from cardiolipin synthase mutant flies (Δ*CLS*). Lipids were extracted from an aliquot corresponding to 2 mg mitochondrial protein and separated by 2-D thin-layer chromatography on silica gel 60 plates developed by chloroform-methanol-20% ammonia (65-30-5) in the first dimension (*vertical*) and chloroform-acetone-methanol-acetic acid-water (50-20-10-10-5) in the second dimension (*horizontal*). Lipids were stained with iodine vapor and phospholipids were determined by colorimetric assay of phosphorus after ashing and expressed as percent of total phospholipid. Mutation of cardiolipin synthase decreases cardiolipin in favor of phosphatidylglycerol. *CL*, cardiolipin; *LPC*, lysophosphatidylcholine; *PA*, phosphatidic acid; *PC*, phosphatidylcholine; *PE*, phosphatidylethanolamine; *PG*, phosphatidylglycerol; *PI*, phosphatidylinositol; *PS*, phosphatidylserine; *Tr*, trace; *ND*, not detected.

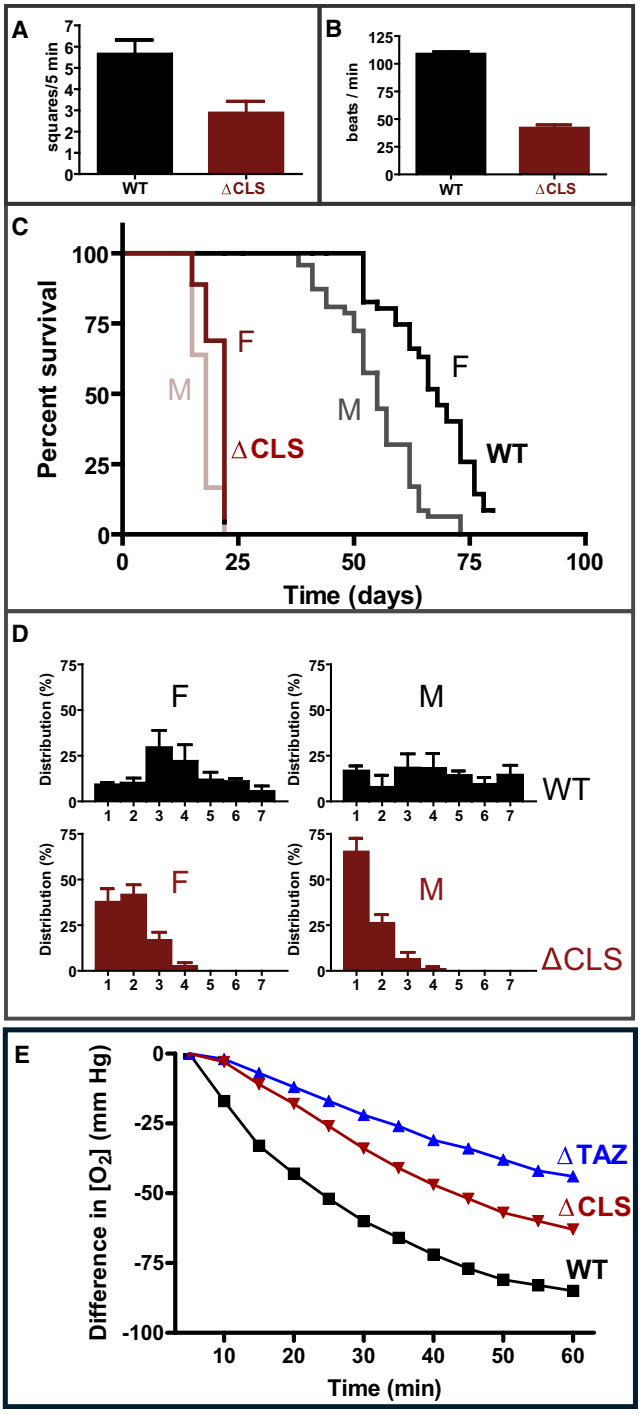

FIGURE 4 Mutation of cardiolipin synthase affects *Drosophila* physiology at all developmental stages. Physiologic variables were determined in the wild-type strain (*WT*) and in the mutant strain (Δ*CLS*). (*A*) Locomotor activities of larvae were measured by the number of squares (0.25 × 0.25 in^2) crossed within 5 min ($N = 9$ in each group). (*B*) Pupal heart rates were determined under a light microscope ($N = 8$ in each group). (*C*) Longevities of adult flies were compared in a Kaplan-Meier graph ($N = 50$ in each group). (*D*) Climbing activities of adult flies (10 days old) were determined by the distance flies climbed within 12 seconds. The graphs show distributions of fly populations over the distance (expressed in 0.5-in units) they climbed within 12 s (triplicate measurements, each performed with 40 flies). (*E*) Respiratory activities of *Drosophila* mitochondria (*WT*, wild-type; Δ*CLS*, cardiolipin synthase mutant; Δ*TAZ*, tafazzin mutant) were measured with the BD Oxygen Biosensor System (BD Biosciences, Franklin Lakes, NJ) according to the specifications of the manufacturer. Mitochondria were incubated at a concentration of 1 mg protein/ml in a medium containing 250 mM sucrose, 15 mM KCl, 1 mM EGTA, 5 mM $MgCl_2$, 30 mM KH_2PO_4, 7 mM succinate, and 2 mM ADP, pH 7.4. Data are the means of two independent experiments. Cardiolipin deficiency is associated with low respiratory activity in ΔTAZ and ΔCLS. *F*, female; *M*, male.

respiratory activity of isolated ΔCLS mitochondria was diminished in comparison to wild-type mitochondria and the loss of cardiolipin had profound effects on fly physiology at all developmental stages, such as reduced locomotor activity at the larval stage, a lower heart rate at the pupal stage, and a shortened life span and reduced climbing activity at the adult stage (Fig. 4). In short, the lack of cardiolipin caused mitochondrial dysfunction, which led to cardiac insufficiency, motor weakness, and early death.

The physiologic decline was accompanied by alterations in mitochondrial ultrastructure and by re-organization of ATP synthase complexes. Many mitochondria in flight muscle and heart muscle showed abnormal morphology (Fig. S5) and this was also observed in isolated mitochondria (Fig. S1). As reported before (20), aggregation of inner membranes was the most common structural abnormality (Fig. S1 and Fig. S5). However, ΔCLS mitochondria with normal morphology were present as well (Fig. S1 *L*) and we were able to derive fragments with normal overall shape to analyze the spatial distribution of ATP synthase particles (Table 1). The effect of cardiolipin deficiency on the structural organization of ATP synthase can be readily appreciated by visual inspection of the 3-D graphs in Fig. 5. In these graphs, F_1 particles are presented as nodes interconnected by line segments. These line segments identify F_1-F_1 pairs closer than 27 nm. The graphs show reduced pairings in the mutant and Fig. 2 confirms that the average number of neighbors dropped from 4 in the wild-type to 2–3 in the mutant. Furthermore, we investigated the oligomerization of ATP synthase by 2D-BN/SDS-PAGE (Fig. 6). Whereas in wild-type mitochondria more ATP synthase was recovered as dimer than as monomer, in ΔCLS, mitochondria ATP synthase migrated mostly, although not exclusively, as monomer. The low number of dimers in 2D-BN/SDS-PAGE of ΔCLS (Fig. 6) seemed to contradict the tomography data that suggested there were 2–3 neighbors/F_1 particle (Fig. 2). However, cryoelectron tomography analyzed isolated crista vesicles that were released by mild sonication, whereas 2D-BN/SDS-PAGE analyzed the entire mitochondrial preparation, including aggregated membranes and other abnormal structures (Fig. S1). In that sense, tomography probably indicated subtle changes induced by cardiolipin deficiency in cristae that retained their normal shape, whereas 2D-BN/SDS-PAGE indicated global changes in all mitochondrial membranes. Since a previous study in yeast did not show any effect of cardiolipin on ATP synthase

TABLE 1 Characteristics of ATP synthase distribution in mitochondrial membrane vesicles derived from flight muscles of different *Drosophila* strains

Strain	Number of vesicles analyzed	Range of vesicle diameters(nm)	Range of vesicle thickness(nm)	Number of F_1 particles analyzed	Percentage of F_1 particles at high-curvature zone	Density of F_1 particles at high-curvature zone (/1000 nm^2)
WT	9	50–250	40–80	646	90 ± 3	3.07 ± 0.38
ΔCLS	9	50–160	50–80	386	82 ± 3	1.70 ± 0.29
ΔTAZ	5	80–250	80–90	462	77 ± 3	1.81 ± 0.27

Data are represented as the mean ± SE. Differences between mutant and wild-type are statistically significant ($P < 0.05$).

dimerization (11), the response to cardiolipin deficiency may be cell-specific and may perhaps be related to the extent of membrane disintegration. In any event, we concluded that the lack of cardiolipin reduced the degree of oligomerization of ATP synthase, which was supported by both 2D-BN/SDS-PAGE (Fig. 6) and cryoelectron tomography (Figs. 2 and 5).

Next, we measured the density of ATP synthase at the high-curvature rim of the vesicles (Table 1). Lack of cardiolipin reduced the density of F_1 particles at the high-curvature rim of vesicles by almost half. The reduced density of F_1 particles was observed not only in disc-shaped vesicles but also in tubular ones (Fig. S6), suggesting that it affected all membrane areas with high intrinsic curvature. However, the overall abundance of ATP synthase relative to other mitochondrial proteins, measured by quantitative Western blotting, was unchanged (Fig. S7). We concluded that the reduced ATP synthase density at high-curvature zones was caused by a redistribution of the enzyme into other membrane zones, such as flat membrane segments and aggregated membranes.

We also studied another *Drosophila* strain, in which cardiolipin deficiency was caused by mutation of TAZ. This mutant had ~80% reduction in the cardiolipin concentration and a change in the molecular composition of cardiolipin (19). In contrast to the ΔCLS mutation, which increased phosphatidylglycerol, the ΔTAZ mutation resulted in an increase in monolysocardiolipin (20). Nevertheless, both the ΔTAZ mutation and the ΔCLS mutation had similar effects on mitochondrial morphology (Fig. S1 and Fig. S5) and on the supramolecular organization of ATP synthase (Figs. 2 and 5). As in ΔCLS, the total amount of ATP synthase was not affected in ΔTAZ (Fig. S7), but the monomer-dimer distribution in ΔTAZ was between those of wild-type and ΔCLS (Fig. 6). The fact that the tomographic data were similar in ΔCLS and ΔTAZ, whereas the 2D-BN/SDS-PAGE data were not, confirms that the two techniques study different populations of molecules. We suggest that 2D-BN/SDS-PAGE analyzed the entire pool of ATP synthase present in the mitochondrial preparation, whereas cryoelectron tomography analyzed ATP synthase selectively in nondegenerated, presumably functional mitochondrial membranes. In conclusion, analysis of two independent cardiolipin depletion mutants (ΔCLS and ΔTAZ) demonstrated that the

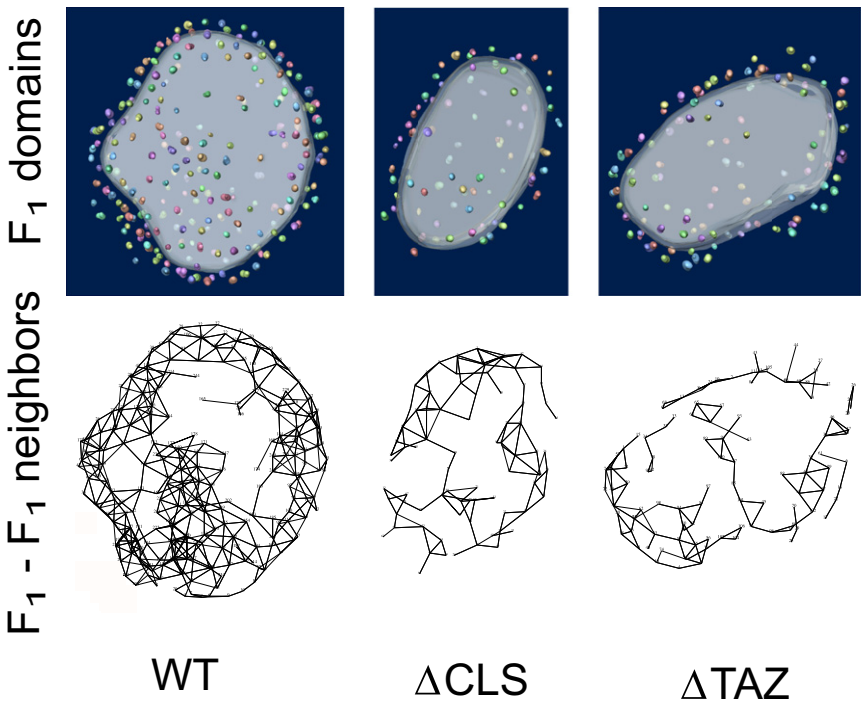

FIGURE 5 Disarray in the supramolecular assembly of ATP synthase in *Drosophila* mutants with cardiolipin deficiency. (*Upper*) 3-D models of membrane vesicles from flight-muscle mitochondria of wild-type flies (*WT*), cardiolipin synthase mutant flies (Δ*CLS*), and tafazzin mutant flies (Δ*TAZ*). The lower panel shows corresponding 3-D models, in which neighbors are connected by lines. A particle is considered the neighbor of another particle if their distance from each other is within 27 nm and if there is no other particle in between the two. The models show less connectivity in the supramolecular structure of ATP synthase in the cardiolipin mutants.

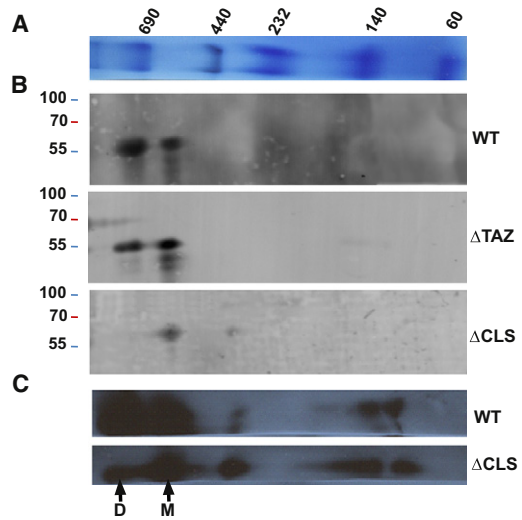

FIGURE 6 2D-BN/SDS-PAGE analysis of ATP synthase in *Drosophila* mitochondria including wild-type (*WT*), cardiolipin synthase mutant (Δ*CLS*), and tafazzin mutant (Δ*TAZ*). (*A*) BN-PAGE molecular weight markers. The molecular mass of markers is given in kDa. (*B*) 2D-BN/SDS-PAGE analysis of the α-subunit of ATP synthase using fluorescing secondary antibody from Li-Cor. In the WT, most of ATP synthase was recovered as dimer (*D*); in ΔTAZ about equal proportions of ATP synthase were recovered as dimer and as monomer (*M*); and in ΔCLS most of ATP synthase was recovered as monomer. (*C*) 2D-BN/SDS-PAGE analysis of the α-subunit of ATP synthase using horseradish peroxidase-conjugated secondary antibody. Some dimers remain present in the ΔCLS mutant.

presence of cardiolipin is critical for the supramolecular organization of ATP synthase.

DISCUSSION

It has been proposed that the oligomeric state of ATP synthase plays a role in crista formation and morphology (15,34). Specifically, it is now widely accepted that dimerization of ATP synthase induces bending of the inner mitochondrial membrane and that further oligomerization of the dimers can provide structural support to extended high-curvature membrane folds (15). Although a number of protein candidates have been identified (35), the molecular mechanism of ATP synthase oligomerization is still not completely understood. Our findings suggest that the lipid composition, specifically the presence of cardiolipin, is also important for oligomerization.

How does cardiolipin promote the ribbonlike assembly of ATP synthase dimers? The effect of cardiolipin could either result from direct interaction with the enzyme or from physical constraints associated with membrane curvature. Cardiolipin is known to partition into high-curvature membrane segments due to its molecular shape (36) and it is thought to adopt a specific orientation with respect to the intrinsic curvature due to its inherent anisotropy (37). We propose that cardiolipin and ATP synthase act in concert to reduce the free energy imposed by membrane curvature, together stabilizing these high-curvature folds.

To quantify the effect of cardiolipin on the structural order in ATP synthase assemblies, we performed a statistical analysis of dimer orientation using the von Mises model (38). Fig. 7 *A* depicts possible states of a population of dimers in a membrane segment, ranging from random distribution to an ideal dimer row (*left* to *right*). For each state, the orientation of dimers yields a population of angles, θ_i, by which dimers deviate from the mean direction. If the

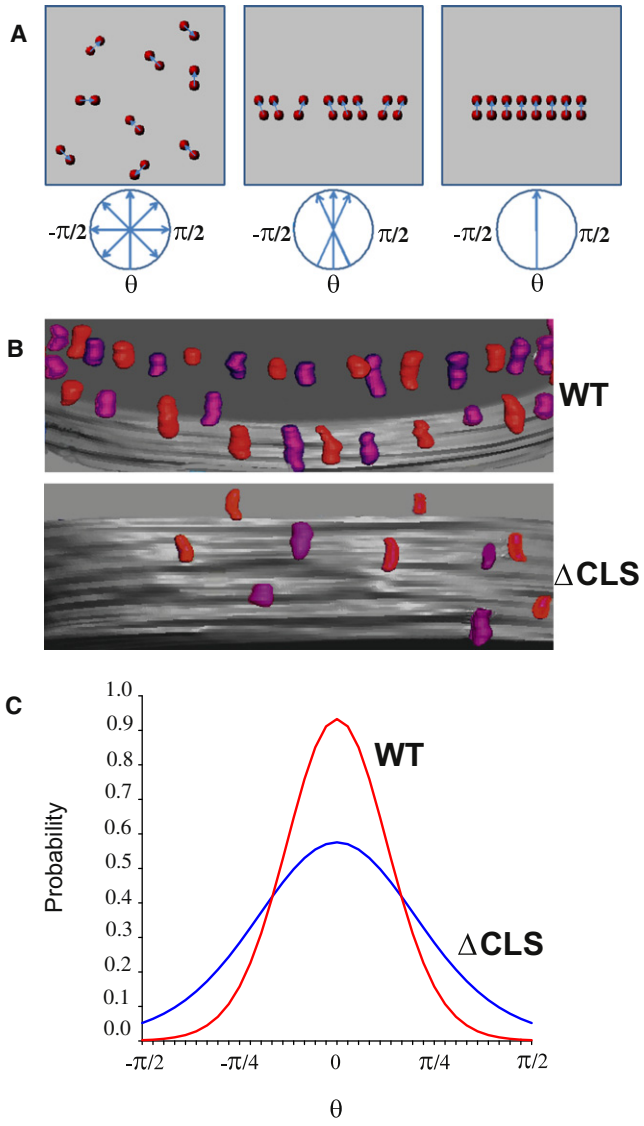

FIGURE 7 Structural order in ATP synthase oligomers. (*A*) Cartoon depicting the orientation of ATP synthase dimers in the membrane plane. The three scenarios include random distribution of isolated dimers (*left*), nonideal dimer row (*middle*), and ideal dimer row (*right*). θ is the angle by which the dimer orientation deviates from the mean direction. (*B*) Tomographic models of dimer rows in wild-type (*WT*) and cardiolipin synthase mutant (Δ*CLS*). (*C*) Probability density functions. Dimer orientations were measured in tomographic models from WT ($n = 75$) and ΔCLS ($n = 34$), yielding a set of angles (θ_1, θ_2,…, θ_n). The sets were used to estimate the concentration parameters using Eq. 2. The concentration parameters were $\kappa = 6.1$ for WT and $\kappa = 2.4$ for ΔCLS. The, probability density functions were calculated from the concentration parameters using Eq. 1.

distribution of the population is normal, the probability density function takes the form (Eq.1):

$$f(\theta,\kappa) = \frac{e^{\kappa\cos\theta}}{2\pi I_0(\kappa)}, \quad (1)$$

where κ is the concentration parameter of the von Mises distribution, and I_0 and I_1 stand for the modified Bessel functions of the first kind, orders 0 and 1, respectively (38). The concentration parameter κ can be estimated by solving Eq. 2:

$$\frac{I_1(\kappa)}{I_0(\kappa)} = \frac{1}{n}\sqrt{\left(\sum_{i=1}^{n}\cos\theta_i\right)^2 + \left(\sum_{i=1}^{n}\sin\theta_i\right)^2}. \quad (2)$$

We determined relative dimer orientations in tomographic models from wild-type and ΔCLS mitochondria. Visual inspection already shows that neighboring dimers were much better aligned in the wild-type (Fig. 7 *B*). The calculated probability density functions confirmed that the dimers in the wild-type were distributed over a much narrower range of angles than in ΔCLS (Fig. 7 *C*). These calculations demonstrate that the presence of cardiolipin in the mitochondrial membrane not only increases the degree of oligomerization of ATP synthase, but also reduces the degree of disorder within the ATP synthase assemblies, promoting the formation of extended dimer rows.

In summary, we demonstrated that cardiolipin molecules play a role in the supramolecular organization of ATP synthase, which is likely to affect crista morphology (15,34) and energy efficiency (18). When comparing ΔCLS and ΔTAZ, we found a correlation between the concentration of cardiolipin and the severity of the phenotype (compare Fig. 4 with data from Schlame and colleagues (19,20), as well as the degree of dimerization of ATP synthase (Fig. 6). On the other hand, ΔCLS and ΔTAZ mutations had a similar effect on the spatial distribution of ATP synthase in membrane vesicles (Figs. 2 and 5 and Table 1). These observations are consistent with the following two-stage model of molecular pathology in cardiolipin mutants: Initially, the lack of cardiolipin creates subtle disturbances in the lateral organization of the membrane in both ΔCLS and ΔTAZ, specifically affecting oligomerization and supramolecular order of the ATP synthase. Then, this process sets the stage for membrane failure, i.e., loss of function and subsequent aggregation of inner membranes, which appears to be more pronounced in ΔCLS, where cardiolipin deficiency is more severe.

SUPPORTING MATERIAL

Seven figures and a movie are available at http://www.biophysj.org/biophysj/supplemental/S0006-3495(11)00379-1.

This work was supported in part by grants from the National Institutes of Health (HL078788, HL083065, GM071044, and 1UL1RR029893) and the Barth Syndrome Foundation. Electron tomography relied on the facilities at the New York Structural Biology Center, which is a STAR center supported by the New York State Office of Science, Technology and Academic Research. Other electron microscopy experiments were done at the New York University Langone Medical Center's Microscopy Core.

REFERENCES

1. Claypool, S. M. 2009. Cardiolipin, a critical determinant of mitochondrial carrier protein assembly and function. *Biochim. Biophys. Acta.* 1788:2059–2068.
2. Klingenberg, M. 2009. Cardiolipin and mitochondrial carriers. *Biochim. Biophys. Acta.* 1788:2048–2058.
3. Mileykovskaya, E., and W. Dowhan. 2009. Cardiolipin membrane domains in prokaryotes and eukaryotes. *Biochim. Biophys. Acta.* 1788: 2084–2091.
4. Schlame, M., and M. Ren. 2009. The role of cardiolipin in the structural organization of mitochondrial membranes. *Biochim. Biophys. Acta.* 1788:2080–2083.
5. Beyer, K., and M. Klingenberg. 1985. ADP/ATP carrier protein from beef heart mitochondria has high amounts of tightly bound cardiolipin, as revealed by ^{31}P nuclear magnetic resonance. *Biochemistry.* 24:3821–3826.
6. Eble, K. S., W. B. Coleman, …, C. C. Cunningham. 1990. Tightly associated cardiolipin in the bovine heart mitochondrial ATP synthase as analyzed by ^{31}P nuclear magnetic resonance spectroscopy. *J. Biol. Chem.* 265:19434–19440.
7. Beyer, K., and B. Nuscher. 1996. Specific cardiolipin binding interferes with labeling of sulfhydryl residues in the adenosine diphosphate/adenosine triphosphate carrier protein from beef heart mitochondria. *Biochemistry.* 35:15784–15790.
8. Zardeneta, G., and P. M. Horowitz. 1993. Physical characterization of a reactivatable liposome-bound rhodanese folding intermediate. *Biochemistry.* 32:13941–13948.
9. Jiang, F., M. T. Ryan, …, M. L. Greenberg. 2000. Absence of cardiolipin in the crd1 null mutant results in decreased mitochondrial membrane potential and reduced mitochondrial function. *J. Biol. Chem.* 275:22387–22394.
10. Zhang, M., E. Mileykovskaya, and W. Dowhan. 2002. Gluing the respiratory chain together. Cardiolipin is required for supercomplex formation in the inner mitochondrial membrane. *J. Biol. Chem.* 277:43553–43556.
11. Pfeiffer, K., V. Gohil, …, H. Schägger. 2003. Cardiolipin stabilizes respiratory chain supercomplexes. *J. Biol. Chem.* 278:52873–52880.
12. Claypool, S. M., Y. Oktay, …, C. M. Koehler. 2008. Cardiolipin defines the interactome of the major ADP/ATP carrier protein of the mitochondrial inner membrane. *J. Cell Biol.* 182:937–950.
13. Ma, L., F. M. Vaz, …, M. L. Greenberg. 2004. The human TAZ gene complements mitochondrial dysfunction in the yeast taz1Delta mutant. Implications for Barth syndrome. *J. Biol. Chem.* 279:44394–44399.
14. Arnold, I., K. Pfeiffer, …, H. Schägger. 1998. Yeast mitochondrial F1F0-ATP synthase exists as a dimer: identification of three dimer-specific subunits. *EMBO J.* 17:7170–7178.
15. Paumard, P., J. Vaillier, …, J. Velours. 2002. The ATP synthase is involved in generating mitochondrial cristae morphology. *EMBO J.* 21:221–230.
16. Allen, R. D., C. C. Schroeder, and A. K. Fok. 1989. An investigation of mitochondrial inner membranes by rapid-freeze deep-etch techniques. *J. Cell Biol.* 108:2233–2240.
17. Buzhynskyy, N., P. Sens, …, S. Scheuring. 2007. Rows of ATP synthase dimers in native mitochondrial inner membranes. *Biophys. J.* 93:2870–2876.
18. Strauss, M., G. Hofhaus, …, W. Kühlbrandt. 2008. Dimer ribbons of ATP synthase shape the inner mitochondrial membrane. *EMBO J.* 27:1154–1160.
19. Xu, Y., M. Condell, …, M. Schlame. 2006. A *Drosophila* model of Barth syndrome. *Proc. Natl. Acad. Sci. USA.* 103:11584–11588.

20. Acehan, D., Z. Khuchua, …, M. Schlame. 2009. Distinct effects of tafazzin deletion in differentiated and undifferentiated mitochondria. *Mitochondrion.* 9:86–95.

21. Lowry, O. H., N. J. Rosebrough, …, R. J. Randall. 1951. Protein measurement with the Folin phenol reagent. *J. Biol. Chem.* 193: 265–275.

22. Winkler, H. 2007. 3D reconstruction and processing of volumetric data in cryo-electron tomography. *J. Struct. Biol.* 157:126–137.

23. Bligh, E. G., and W. J. Dyer. 1959. A rapid method of total lipid extraction and purification. *Can. J. Biochem. Physiol.* 37:911–917.

24. Schlame, M. 2007. Assays of cardiolipin levels. *Methods Cell Biol.* 80:223–240.

25. Sun, G., K. Yang, …, R. W. Gross. 2008. Matrix-assisted laser desorption/ionization time-of-flight mass spectrometric analysis of cellular glycerophospholipids enabled by multiplexed solvent dependent analyte-matrix interactions. *Anal. Chem.* 80:7576–7585.

26. Wittig, I., H.-P. Braun, and H. Schägger. 2006. Blue native PAGE. *Nat. Protoc.* 1:418–428.

27. Sohal, R. D. 1975. Mitochondrial changes in flight muscles of normal and flightless *Drosophila melanogaster* with age. *J. Morphol.* 145: 337–353.

28. Nicastro, D., A. S. Frangakis, …, W. Baumeister. 2000. Cryo-electron tomography of neurospora mitochondria. *J. Struct. Biol.* 129:48–56.

29. Dudkina, N. V., G. T. Oostergetel, …, E. J. Boekema. 2010. Row-like organization of ATP synthase in intact mitochondria determined by cryo-electron tomography. *Biochim. Biophys. Acta.* 1797:272–277.

30. Rabl, R., V. Soubannier, …, A. S. Reichert. 2009. Formation of cristae and crista junctions in mitochondria depends on antagonism between Fcj1 and Su e/g. *J. Cell Biol.* 185:1047–1063.

31. Ohtsuka, T., M. Nishijima, …, Y. Akamatsu. 1993. Mitochondrial dysfunction of a cultured Chinese hamster ovary cell mutant deficient in cardiolipin. *J. Biol. Chem.* 268:22914–22919.

32. Jiang, F., Z. Gu, …, M. L. Greenberg. 1999. Cardiolipin synthase expression is essential for growth at elevated temperature and is regulated by factors affecting mitochondrial development. *Mol. Microbiol.* 31:373–379.

33. Choi, S. Y., F. Gonzalvez, …, M. A. Frohman. 2007. Cardiolipin deficiency releases cytochrome *c* from the inner mitochondrial membrane and accelerates stimuli-elicited apoptosis. *Cell Death Differ.* 14: 597–606.

34. Allen, R. D. 1995. Membrane tubulation and proton pumps. *Protoplasma.* 189:1–8.

35. Wittig, I., and H. Schägger. 2009. Supramolecular organization of ATP synthase and respiratory chain in mitochondrial membranes. *Biochim. Biophys. Acta.* 1787:672–680.

36. Huang, K. C., R. Mukhopadhyay, and N. S. Wingreen. 2006. A curvature-mediated mechanism for localization of lipids to bacterial poles. *PLOS Comput. Biol.* 2(11, e151):e151.

37. Fournier, J. B., and P. Galatola. 1997. Sponges, tubules and modulated phases of para-antinematic membranes. *J. Phys. II.* 7:1509–1520.

38. Fisher, N. I. 1993. Statistical Analysis of Circular Data. Cambridge University Press, Cambridge, UK.